An effective medium description of 'Swiss Rolls', a magnetic metamaterial

2007 J. Phys.: Condens. Matter 19 456216

(http://iopscience.iop.org/0953-8984/19/45/456216)

IOP PUBLISHING JOURNAL OF PHYSICS: CONDENSED MATTER

J. Phys.: Condens. Matter **19** (2007) 456216 (16pp) doi:10.1088/0953-8984/19/45/456216

An effective medium description of 'Swiss Rolls', a magnetic metamaterial

M C K Wiltshire[1,2], J B Pendry[2], W Williams[2] and J V Hajnal[1]

[1] Imaging Sciences Department, Clinical Sciences Centre, Hammersmith Hospital, Imperial College London, London W12 0NN, UK
[2] The Blackett Laboratory, Department of Physics, Imperial College London, London SW7 2AZ, UK

E-mail: michael.wiltshire@imperial.ac.uk

Received 6 July 2007, in final form 24 September 2007
Published 15 October 2007
Online at stacks.iop.org/JPhysCM/19/456216

Abstract

The 'Swiss Roll' metamaterial medium is well suited to operation in the radio frequency (RF) range, because it has a low resonant frequency and a strong magnetic response. Two prisms of this material, one hexagonal and one square, have been constructed and characterized both at the metamaterial's resonant frequency of 21.5 MHz and above it, where the effective permeability is strongly negative. A series of spatial resonances is observed in the field patterns on the surfaces of the prisms. Using an effective medium description, we have carried out both analytical and numerical modelling of the electromagnetic behaviour of the metamaterial, and find, within certain obvious limitations, extremely good agreement between the measured and modelled results.

(Some figures in this article are in colour only in the electronic version)

1. Introduction

Metamaterials [1–3] can provide an engineered response to electromagnetic radiation that is not available from the range of naturally occurring materials. They consist of arrays of structures in which both the individual elements and the unit cell are small compared to the wavelength of operation; homogenization of the structures then allows them to be described by the conventional electromagnetic constants of permittivity (ε) and permeability (μ), but with values that could not previously be obtained. For example, materials with simultaneously negative ε and μ can be built that have a negative refractive index [4–6], and much attention has been given to the behaviour of such media [7].

In much of the above work, the magnetic medium has consisted of split ring resonators (SRR) [3]. These are simple to fabricate [8] and are active in the microwave regime, providing negative permeability typically over a bandwidth of some 10% [9]. At lower frequencies, however, they become impractically large, and the sparseness of their packing reduces their

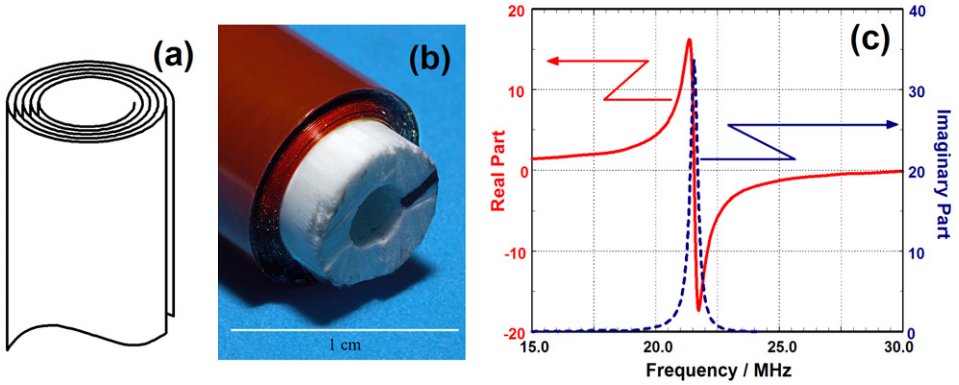

Figure 1. Schematic of a Swiss Roll (a) and a photograph (b) of a typical roll used in the experiments at 21.5 MHz. The measured real (red full line and left axis) and imaginary (blue dashed line and right axis) parts of the permeability of a Swiss Roll as a function of frequency are shown in (c).

effectiveness. Another structure, the so-called Swiss Roll [3], is much better suited to lower-frequency operation. This material, which is an array of elements consisting of a spiral-wound conductor on a cylindrical mandrel (figures 1(a) and (b)), exhibits a resonant frequency in the megahertz range (typically 10–100 MHz) and is a much stronger magnetic medium, exhibiting negative permeability over a bandwidth that may be 40% of the resonant frequency (figure 1(c)).

Because the frequency of operation is so low, the wavelength of the electromagnetic radiation is extremely long, and the condition that the structure should be much smaller than a wavelength is easily met. For example, we have previously described [10–12] Swiss Roll material operating at 21.5 MHz for which $\lambda/a > 1000$ (where a is the unit cell size and λ is the wavelength). This should be compared to the $\lambda/a \approx 5$ that can be achieved with the SRR structure. A further aspect of working at low frequency is that all distances are very small compared to the wavelength, so all measurements are made in the very near field, where the electric and magnetic fields are essentially decoupled [13], thus simplifying both the material requirements and the interpretation of measurements.

The material is also highly anisotropic, and the combination of a large permeability and strong anisotropy with very long wavelength leads to exotic propagation modes. In a previous paper [11], we showed that, on resonance, a prism of the metamaterial behaved as a magnetic endoscope, transferring faithfully a magnetic field pattern from one side to the other. In this paper, we concentrate on the frequency regime above resonance, where the effective permeability is negative.

As mentioned above, there has been great interest in the behaviour of so-called negative materials. However, the anisotropy of the present system renders it quite different from the negative media that give rise to focussing and sub-wavelength imaging [13–18]: these require the refractive index to be isotropic. Anisotropic or indefinite media [19, 20] have different characteristics. There are also analogies with plasmonic systems: in the very near field the electric and magnetic fields are equivalent, so one might expect the material to behave as a magnetic plasma, displaying the plasmon resonances characteristic of metallic nanoparticles in an electric field [21], with the propagation of radiation being characterized by conical wavefronts through an anisotropic plasma [22, 23] rather than by conventional dispersion.

Accordingly, in this paper we investigate the behaviour of the highly anisotropic Swiss Roll medium in the negative permeability regime. In previous reports [11, 12, 24, 25] we have described the appearance of resonant field patterns on the surface of a prism of

metamaterial; these we interpreted using the effective medium approach and achieved some qualitative understanding of the data. In this paper, we extend these methods in an attempt to provide a quantitative model. However, this approach has only provided a partially successful description of the observed phenomena, so we have used numerical modelling to test the effective medium description. In the next section we describe the development of the material and the measurements, and summarize the experimental results. In section 3, we describe the analytical model, and then describe how we have used a commercial numerical simulation package, CST MicroWave Studio[3], to perform the calculations. In section 4, we make a detailed comparison of the calculated results to the measured results, and find excellent agreement between the numerical simulation and the measurements. In the final section, we consider the limitations of the models and review an alternative, microscopic description of a metamaterial as an array of coupled resonators [26–30]. This approach gives good agreement with the observed field patterns, but also has its limitations, which complement those of the effective medium model. We conclude that the effective medium description, within certain obvious limitations, provides an extremely accurate model of the metamaterial.

2. Experimental details

2.1. Material development

'Swiss Rolls' [3] (figure 1) are particularly suitable for use as metamaterial elements up to ∼100 MHz, because they have inherently large self-inductance and self-capacitance, and so a low resonant frequency for their size. The magnetic permeability of an array of such rolls as a function of frequency, f, is given by [11]

$$\mu_{xx} = \mu_{yy} = 1; \qquad \mu_{zz}(f) = \mu'_{zz} + \mathrm{i}\mu''_{zz} = 1 - \frac{F}{(1 - f_0^2/f^2) + \mathrm{i}\gamma/f}, \quad (1)$$

where F is the filling factor, f_0 is the resonant frequency, and γ represents the damping or loss. This form of the permeability naturally falls into three segments: at frequencies below the resonance, $f < f_0$, the real part of the permeability, μ'_{zz} is positive; between the resonance and the magnetic equivalent of the plasma frequency, $f_\mathrm{p} = f_0/\sqrt{(1-F)}$ where $\mu'_{zz} = 0$, μ'_{zz} is negative; and at yet higher frequency, $f > f_\mathrm{p}$, μ'_{zz} is small and positive.

We have made Swiss Rolls with a $Q \sim 60$ at a resonant frequency near 21.5 MHz, by rolling approximately 11 turns of the material Espanex® SC-18-12-00-FR[4], which consists of an adhesiveless laminate of an 18 μm copper sheet with a 12.5 μm polyimide layer, onto a 10 mm diameter Delrin® mandrel. The effective permeability of the Swiss Roll medium was determined by inserting a roll into a long solenoid, and measuring the changes in the complex impedance that result. Corrections for the partial volume and demagnetization were applied, and hence the real and imaginary parts of the effective permeability were determined [11]. A typical plot for the permeability is shown in figure 1(c). On resonance a peak value of $\mu''_{zz} = 35$ is found. Data from these measurements were used to determine the parameters in (1), giving $f_0 = 21.55$ MHz, $\gamma = 0.35$ and $F = 0.56$.

Over 300 rolls, each 50 mm long, were made, with their resonant frequencies centred on 21.5 MHz. Although nominally identical, in practice there was a distribution of frequencies significantly greater than the width of any individual resonance, so it was necessary to tune each roll to the correct resonant frequency. Tuning was carried out by adding a capacitively coupled sleeve that extended 10 mm beyond the end of the roll [11]. 271 tuned rolls were

[3] CST GmbH, Darmstadt, Germany.
[4] Nippon Steel Chemical Company, Tokyo, Japan.

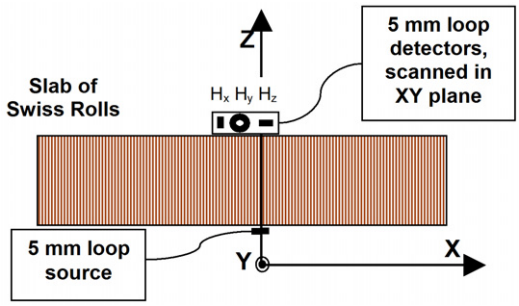

Figure 2. Schematic layout of the scanning experiment. A 5 mm diameter source loop is placed behind the slab, oriented along the axis (OZ). The detectors (a set of 5 mm loops) were scanned in the XY plane to measure the transmitted field components H_x, H_y, H_z just above the output face.

assembled as a hexagonal array in a balsawood box to create a prism of material, which had 200 mm long diagonals and was 60 mm thick [11]. Another prism was made by packing 289 rolls into a square box of side 192 mm [25], with the square packing being maintained by placing appropriately sized wooden spacers at the interstices between the rolls.

It should be noted that the value of the filling factor given above is the effective value that would be obtained if the rolls could fill all space, i.e. the volume correction was just the ratio of the measuring coil volume to the roll volume. In reality, of course, the rolls do not fill space and we expect a lower value of F to apply. When the rolls are assembled into the prisms, the filling factor F is reduced, by a factor of $\pi/(2\sqrt{3})$ for the hexagonal prism or $\pi/4$ for the square prism, leading to $F = 0.51$ and $F = 0.44$, respectively.

2.2. Measurements

To measure the magnetic properties of the prisms, we placed a small magnetic dipole source (a 5 mm diameter loop) centrally on the base of the box containing the prism, some 5 mm away from the end of the rolls, and oriented so that its axis was parallel to the axis of the Swiss Rolls. Similar loops, oriented to receive the x-, y-, and z-components of the transmitted field, were scanned in the XY plane, about 5 mm above the surface of the Swiss Rolls, and in the XZ plane of the output space. A schematic of the layout is shown in figure 2.

The source and detector loops were connected to a network analyser that recorded the signal as a function of frequency in the range 15–35 MHz, thus spanning the magnetically active frequency range. The data were processed to provide maps of the axial field (H_z) and the transverse (H_t) or radial ($H_\mathrm{r} = \sqrt{H_x^2 + H_y^2}$) field (for the square and hexagonal prism, respectively) in the measurement plane at each frequency.

2.3. Results

Some of the results have been presented previously [11, 12, 24, 25, 31], and they will be discussed in detail in section 4, where they are compared with the results of the modelling. Here, however, we give an overview of the main features, dividing the discussion into the three frequency regions identified in section 2.1.

2.3.1. $f < f_0$. Here, the metamaterial acts as a conventional magnetic material, and a modified dipole field pattern is observed. We find that H_z is a maximum at the centre of the

pattern and falls rapidly away from the centre, whereas H_r or H_t is low at the centre, has a maximum at a diameter of a few millimetres, and then also falls. This variation is confined to a central region 20–30 mm in diameter. As μ'_{zz} increases, this pattern is maintained, with the central peak in H_z increasing in intensity and decreasing in width as the frequency rises towards the resonance. On resonance, we find the narrowest peak for H_z, as was described in our earlier work [11].

2.3.2. $f > f_p$. Here, as for the low-frequency region, the metamaterial acts as a conventional magnetic material, but with a small positive permeability, and a modified dipole field pattern similar to that found for $f < f_0$ is observed. Again, H_z is a maximum at the centre of the pattern and falls rapidly away from the centre, whereas H_r or H_t is low at the centre, has a maximum at a diameter of a few millimetres, and then also falls. Just above f_p, the pattern extends to cover the whole sample, but with increasing frequency it collapses towards a central region, so that by 35 MHz it is some 40 mm in diameter.

2.3.3. $f_0 < f < f_p$. In this region, both prisms displays a sequence of field patterns that appear to correspond to spatial resonances. These all have $H_z = 0$ at the periphery of the prisms, as demanded by the boundary conditions, but their detailed structure depends on both the shape of the prism and its permeability and hence the frequency.

Above f_0, the field pattern rapidly spreads out to cover the whole face of the prism, although the distribution is featureless, and dominated by the strong central peak. By 22.0 MHz, some structure is apparent in the field pattern of both prisms, with a ring of higher intensity developing near the periphery. As the frequency is increased, the pattern consolidates into this outer ring along with further rings of higher intensity within it, reaching a maximum intensity at 22.5 MHz for both prisms.

It is simpler to describe both the patterns and their evolution from this point by considering the sequence as the frequency is reduced from above f_p. As described above, just above f_p the pattern extends across the entire surface and the intensity increases as the frequency is reduced, developing into a broad uniform peak at 28.5 MHz for the square prism and 29.7 MHz for the hexagonal prism. These two frequencies correspond quite closely to the values of f_p derived from the resonant frequency f_0 and the filling factor F for the two cases ($f_p = 28.8$ and 30.7 MHz for the square and hexagon, respectively). Below these frequencies, the overall intensity decreases, falling particularly rapidly in the central region, albeit with a narrow central peak which is presumably due to flux guiding through the central roll. Thus we see a ring of low intensity forming around the central peak. This ring of minimum intensity deepens and expands while the intensity outside it also falls until 27.5 MHz in the hexagon and 26.5 in the square samples. The intensity both at the centre and in the outer regions then starts to rise, with the central region broadening, until both regions reach a maximum intensity at 24.7 MHz in both samples. Here, the square has maxima in the centre and at the four corners, whereas the hexagon has a central maximum and an outer ring of intensity with weak maxima at the corners of the hexagon. As the frequency is reduced further, this sequence is reproduced: the broad central peak develops within itself a ring of low intensity which deepens and expands, driving a second band of high intensity outwards. In the hexagon, this forms another ring, reaching a maximum at 23.2 MHz. The process repeats again, leading to the three-ring pattern becoming fully developed at 22.6 MHz. The case of the square is more complicated, as the rings reform into regions of high intensity at the corners and face centres at 23.65 and 23.25 MHz, and finally into three rings at 22.5 MHz. These patterns are shown in figure 6 (section 4.2.1) for the square prism and figure 7 (section 4.2.2) for the hexagonal prism, respectively, where they are compared with the results of the modelling.

The in-plane fields vary in a similar way, and again it is simpler to describe the sequence as the frequency is reduced from the high end. For the uniform mode, where H_z has a broad maximum at the centre and falls to zero at the edge, the in-plane field H_r or H_t is zero at the centre and is maximum at the periphery. When the frequency is reduced to the first ring pattern, the in-plane field complements the axial field: whereas H_z has a central peak and a ring of intensity in the outer half of the face, H_r is minimum at the centre, has a maximum overlying the region of minimum axial intensity, falls to a minimum and rises again with the opposite in-plane direction towards the periphery. As the frequency is reduced further, the ring patterns continue to complement each other, and the overall field direction appears to rotate towards the periphery, with an increasing number of turns as the frequency is reduced. Once again, the case of the square prism is more complicated, but where there are 'rings' of axial field intensity, the in-plane field complements them.

3. Modelling

3.1. Analytical

In our previous work [11, 12, 24, 25, 31], we treated the material as a homogeneous anisotropic prism of material of thickness d with a magnetic response given by (1), and considered the propagation of electromagnetic waves through the medium. By solving Maxwell's equations in $(\boldsymbol{k}, \omega)$ space, it was shown that the dispersion relation for s-polarized radiation in the (xz) plane was

$$\frac{k_x^2}{\mu_{zz}} + \frac{k_z^2}{\mu_{xx}} = k_0^2 = \frac{\omega^2}{c_0^2}. \tag{2}$$

With $\mu_{xx} = 1$, this becomes

$$k_z^2 = k_0^2 - \frac{k_x^2}{\mu_{zz}}. \tag{3}$$

On resonance, when $|\mu_{zz}| \to \infty$, we see that (3) gives $k_z \approx k_0$, so that all the transverse Fourier components, k_x, of the field are transported with the same wavevector: an input field distribution is faithfully transported to the output face of the prism [11].

The eigenvectors (after removing the redundant factors) are found to be

$$\begin{bmatrix} B_x \\ B_z \end{bmatrix} = \begin{bmatrix} -k_z \\ k_x \end{bmatrix}, \tag{4}$$

so we can match the fields at the boundaries between the prism and free space to obtain the interface transmission and reflection coefficients as a function of the transverse wavevector k_x. Hence the transmission of a semi-infinite slab can be calculated in the conventional manner [32] to obtain

$$B_z(r, z) = 2\pi \int_0^\infty [c_{k_x}^+ J_0(k_x r) \exp(\mathrm{i}k_z(z - d))]\, \mathrm{d}k_x, \tag{5}$$

where

$$c_{k_x}^+ = \left[\cos(k_z d) + \frac{1}{2}\left[\frac{\mu_{xx}k_x}{k_z} - \frac{k_z}{\mu_{xx}k_x}\right]\sin(k_z d)\right]^{-1} \tag{6}$$

is the overall transmission coefficient of semi-infinite slab as a function of k_x and $J_0(k_x r)$ is the zeroth-order Bessel function of the first kind.

In the very near field, $k_x, k_z \gg k_0$, so, away from resonance, (3) reduces to

$$k_z \approx \mathrm{i}k_x/\sqrt{\mu_{zz}}. \tag{7}$$

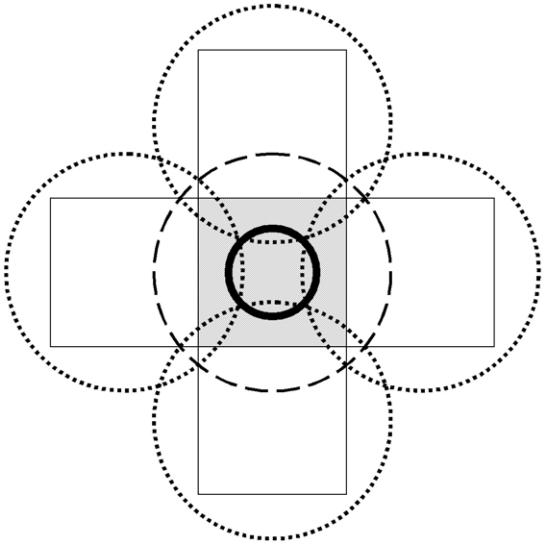

Figure 3. Schematic construction showing the development of the pattern of field intensity at the output surface of the prism. The shaded square represents the prism, and the bold circle the cone of radiation given by equation (8). The dashed circle represents the intensity reflected internally from the input and output faces, leading to a cone with three times the radius of the primary cone, and the dotted circles show that intensity internally reflected from the side walls of the prism.

Thus when $\mu'_{zz} < 0$ and μ''_{zz} is small, k_z remains approximately real for all values of k_x, and the fields propagate through the medium in a conical wavefront [22, 23] with an angle determined by the value of μ_{zz}. Thus a point source at the input face generates a ring of intensity at the output face whose radius is given by

$$r = -d\,\mathrm{Im}(1/\sqrt{\mu_{zz}}). \tag{8}$$

To take into account the finite size of the sample, we note that there are internal reflections at the entrance and exit surfaces, and also at the sides of the material. For the square prism, this can be treated by considering a unit cell with periodic boundary conditions and folding all the higher-order components back into the central zone (see figure 3) to deduce the total field. We combine this with the expressions (5) and (6) for the transmission coefficient to calculate the output pattern, which should consist of a central ring whose radius is given by (8) along with additional structure arising from internal reflections.

3.2. Numerical

We carried out numerical simulations using the transient solver of CST MicroWave Studio® (see footnote 3). Here, a short pulse of radiation is launched into the model, and the evolution of the field distribution is calculated as a function of time. This is then Fourier transformed to provide the frequency response of the system. We modelled the metamaterial prism as a slab of uniform material having an anisotropic, frequency-dispersive permeability. Here, the transverse permeabilities were set to unity, and the axial permeability was described using the Lorentzian dispersion in MicroWave Studio (MWS), which sets

$$\mu(f) = \mu_s + \frac{(\mu_s - \mu_\infty) f_0^2}{(f_0^2 - f^2) - \mathrm{i} f \gamma}, \tag{9}$$

where μ_s and μ_∞ are respectively the low-frequency and high-frequency limiting values of the permeability, f_0 is the resonant frequency and γ is the damping. Comparing this with (1), we see that our metamaterial requires $\mu_s = 1$ and $\mu_\infty = 1 - F$; the resonant frequency and the damping have the same values in both equations.

As discussed in section 2.1, $F = 0.51$ and $F = 0.44$ for the hexagonal and square prisms respectively, so we require $\mu_\infty = 0.49$ or 0.56. However, in-built constraints in MWS prevented us from using these parameters. We retained the measured resonant frequency and damping, kept $\mu_\infty = 1$, and selected a static permeability, μ_s, that gave $\mu'_{zz} = 0$ at the correct frequency. However, it was impossible to achieve an overall match between the measured and modelled permeabilities, and so comparisons could not be based on the absolute frequency but had to be made by identifying the field patterns and their development as a function of frequency.

The source of the magnetic field was modelled as a 5 mm diameter wire loop placed in the space behind the slab and excited by a current source in the loop. The background to the model was vacuum, and so-called 'open' boundaries (i.e. perfectly matched layers) were placed approximately $\lambda/8$ away from the region of interest; this distance was set by the software itself. This led to an extremely large model, but the gridding was required to be fine only across the metamaterial region; away from the material, quite a coarse grid was used. Because the system is highly resonant, the convergence criteria in MWS did not always give consistent results. Therefore, following the excitation pulse of ∼355 ns duration, the calculation was allowed to evolve until no further signal was observed on probe monitors placed in the output space. This took typically 15 pulse widths or about 5500 ns with a run time of typically 30 h on a PC with a 3 GHz processor. Tests were run with different calculation times to ensure that this choice was suitable for the range of models under consideration. The resulting magnetic fields were monitored in a plane 5 mm in front of the slab, as was done in the measurements, and the results were recorded at 0.1 MHz intervals in the range 20–30 MHz. The central region (±100 mm in both X and Y directions) was stored for further processing and comparison with the measured data.

4. Comparison of measured and modelled results

4.1. On resonance

We make the first comparison between the modelled and measured results at the resonant frequency of the individual elements, f_0, when $|\mu|$ becomes large. Then, as shown in section 3.2, the material acts as a coherent face-plate for magnetic flux, and transfers an input field pattern from one side of the prism to the other. This behaviour was observed in our early measurements [11], and was discussed there in terms of the analytical model. Here, we consider whether the numerical model supports our interpretation of the data. In figures 4(a) and (b), we show the measured axial (H_z) field patterns, both in the plane containing the axis (the XZ plane) and in the plane of the output face (the XY plane; see figure 2), that arise from a 5 mm diameter source placed behind the prism. The observed pattern corresponds to that of a dipole lying on the output face—notice the diagonal band of low intensity, characteristic of a dipole field. In this figure, and in the following three figures, blue regions represent low field intensity whereas the red regions denote high intensity. The numerical results are shown in figures 4(c) and (d), for the same planes as for the data, and not only show that an excellent match is obtained in the output space but also reveal the field in the input space and the propagation of the field through the prism. These figures demonstrate convincingly that the face-plate behaviour is obtained in a homogeneous (but strongly anisotropic) effective medium, and is not just due to guiding through the individual Swiss Rolls.

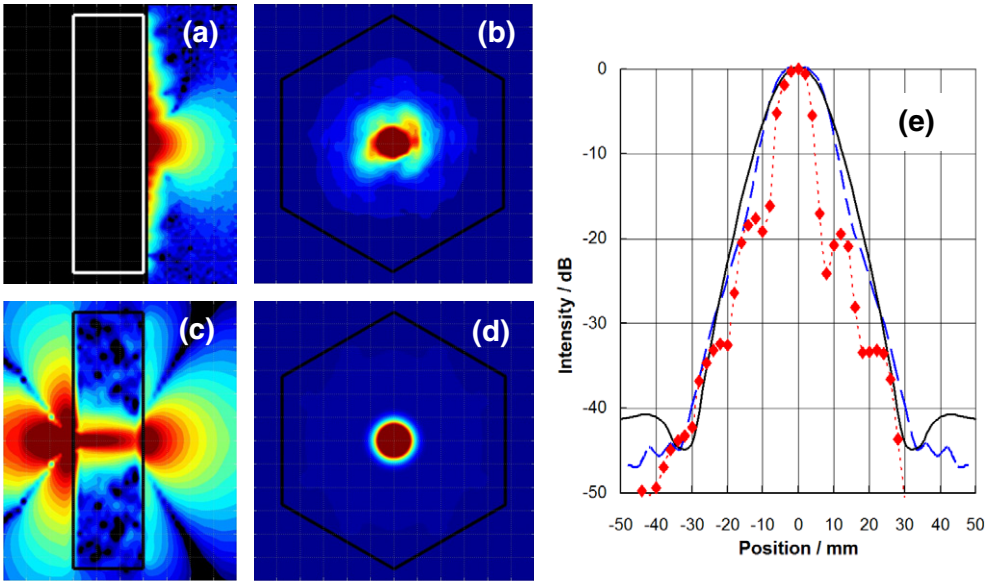

Figure 4. Axial magnetic field (H_z) patterns from the hexagonal prism on resonance: (a) measured intensity (dB) in the XZ plane, and (b) amplitude in the XY plane, 5 mm above the prism; (c) modelled intensity (dB) in the XZ plane, showing the jet of flux propagating through the material, and (d) amplitude in the XY plane, 5 mm from the prism. (e) Comparison of measured and calculated profiles: the points are measured data with the dotted line being a guide to the eye, the dashed line is the analytical profile and the full line is the profile from the numerical calculation. The measured intensity without the prism is about −60 dB [11] (not shown).

Moreover, in figure 4(e), we plot a comparison of the measured profile (points) with the analytic calculation based on the formalism of section 3.1 that we reported previously [11] (dashed line) and the profile obtained from the present numerical calculation (full line). The detailed structure in the measured data arises because, in this measurement, we used a 3 mm diameter probe and sampled at 2 mm steps, thus ensuring that the discrete rolls could be resolved. We see that flux is trapped to some extent inside the individual elements, and clearly this effect cannot be represented in an effective medium approximation. Therefore, the comparison should be made between the envelope of the data points and the calculated profiles. It is clear that the agreement between the two calculated profiles is very good over a wide intensity range (note the logarithmic scale), and both are accurate envelopes for the measured points, so that an anisotropic effective medium model does indeed represent the observed fields correctly.

4.2. Above resonance

As pointed out above, MWS cannot accept the fitted parameters for the permeability in its Lorentzian dispersion model, so the permeability in the model at any given frequency is not the same as that in the experiment. Therefore, rather than being able to make comparisons at the specific, measured frequency points, we have had to consider the sequence of calculated field patterns as a function of frequency, and how one pattern evolves into the next. The first pattern considered in the negative permeability region above the resonant frequency was that found at 24.7 MHz in the square prism. This pattern has high intensity in the central region and in the corners of the square, and is shown in figure 5(a).

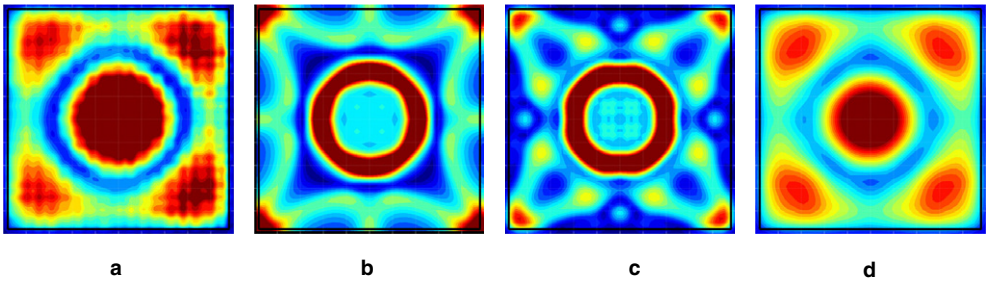

Figure 5. Comparison of H_z field distributions observed 5 mm above the output face of the square prism at 24.7 MHz. (a) The measured result, (b) that from the analytical model, and (c) the numerical simulation, all using a 5 mm diameter source placed 5 mm behind the input face. (d) The result for the numerical model using a plane wave excitation.

The first simulations were made using the same physical layout as the experiment, with the source placed 5 mm behind the slab and the fields monitored 5 mm in front of it. The results on resonance in figure 4 were obtained in this configuration. In figures 5(b) and (c), we show the results of the analytical calculation and the numerical simulation for this configuration that correspond best to the data at 24.7 MHz. We note first that the two calculated distributions are quite similar, although the numerical model shows rather more structure than the analytical calculation. However, it is clear from these plots that the calculated patterns contain much finer detail than was actually observed: the measured features were much larger and more diffuse than the calculated ones.

A further observation is that when a plane wave source is used to illuminate the sample in the numerical simulation, with the magnetic field aligned along OZ and propagation along OX, we obtain the distribution shown in figure 5(d). This gives very good agreement with the measured data.

In part, this difference is a consequence of the finite size of the elements in the metamaterial: no component of the field pattern with a spatial wavelength smaller than the size of an element can be sustained, so there is an effective cut-off at high transverse spatial frequency or wavevector. Moreover, the finite size of the prism itself leads to a minimum for the transverse wavevector. Thus, for accurate modelling, we need to restrict the range of wavevector. We have implemented this in the analytical model with some success, and the results are discussed in the following section. However, it not possible to impose such limits directly in the numerical model, so we have approximated the effect of the upper limit on wavevector by moving the source further away from the prism, thus making the incident field pattern more diffuse and reducing the high spatial frequency components of the input field. When the source is placed 20 mm behind the prism, excellent agreement is obtained with experiment, both for the individual patterns and for their evolution from one to another as a function of frequency. In the following two sections, we discuss the results using this model setup for the two prisms.

4.2.1. The square prism. The measured results for the square prism are shown in the central column of figure 6, once again starting at the highest frequency. As pointed out above, in the negative μ_z regime, the boundary conditions at the edges of the prism require $H_z = 0$. At high frequency (28.5 MHz), we observe a uniform mode (with $H_z = 0$ at the edges). As the frequency is reduced, all intensity fades until the next resonance at 24.7 MHz, discussed above, is approached, when intensity grows both at the centre of the square and at the corners. As the next resonance is approached, the central region grows along the axes, until at 23.75 MHz a pattern of nine high-intensity spots is seen. Increasingly complicated patterns then evolve as the

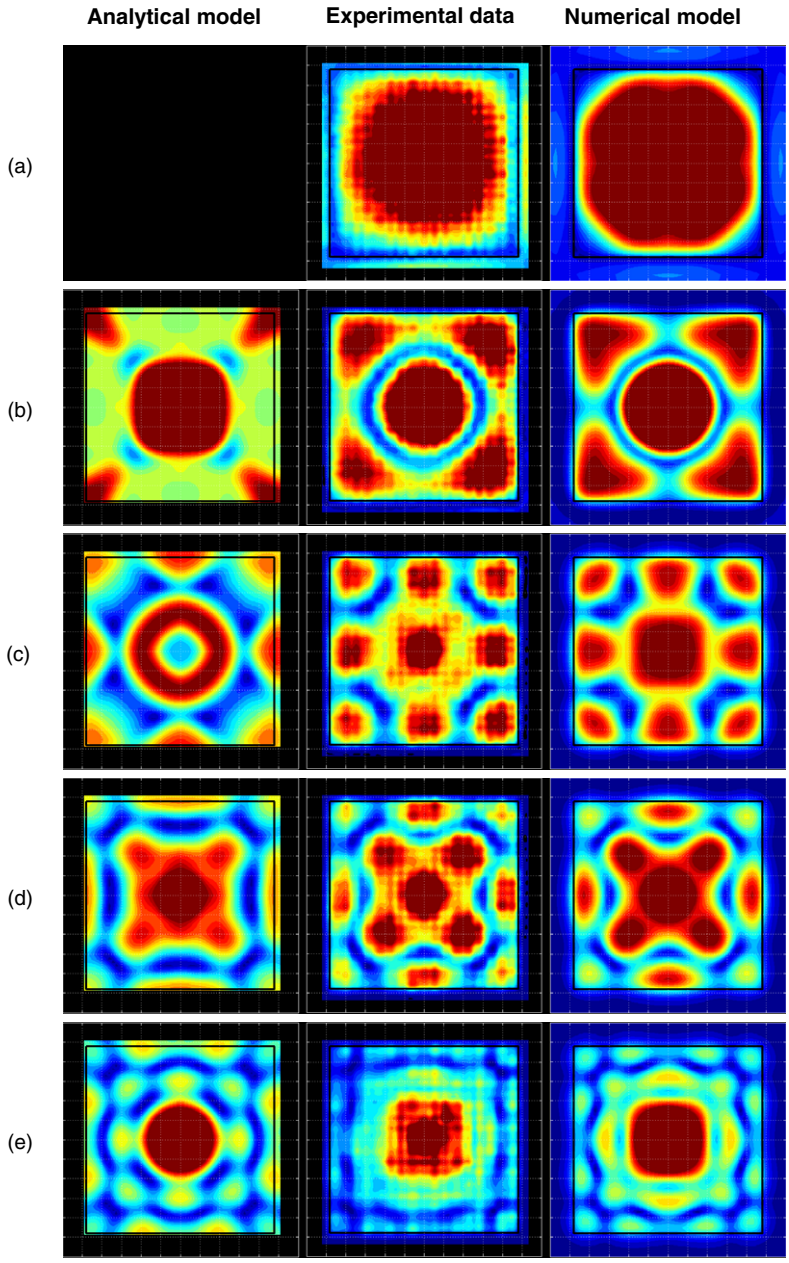

Figure 6. Comparison of (centre column) the field patterns observed 5 mm from the exit face of the square prism at (a) 28.50 MHz, (b) 24.70 MHz, (c) 23.65 MHz, (d) 23.25 MHz, and (e) 22.50 MHz with the patterns calculated using the analytical model (left column) and the numerical model (right column).

frequency is reduced towards f_0; examples are shown in figure 6 for 23.25 and 22.50 MHz. The task of the simulation is to reproduce not only the resonant patterns, but also the progression from one to another. We also note in figure 6 that the measured patterns have a granularity: this is due to the size of the individual elements of the metamaterial and we cannot expect any calculation based on an effective medium model to reproduce this.

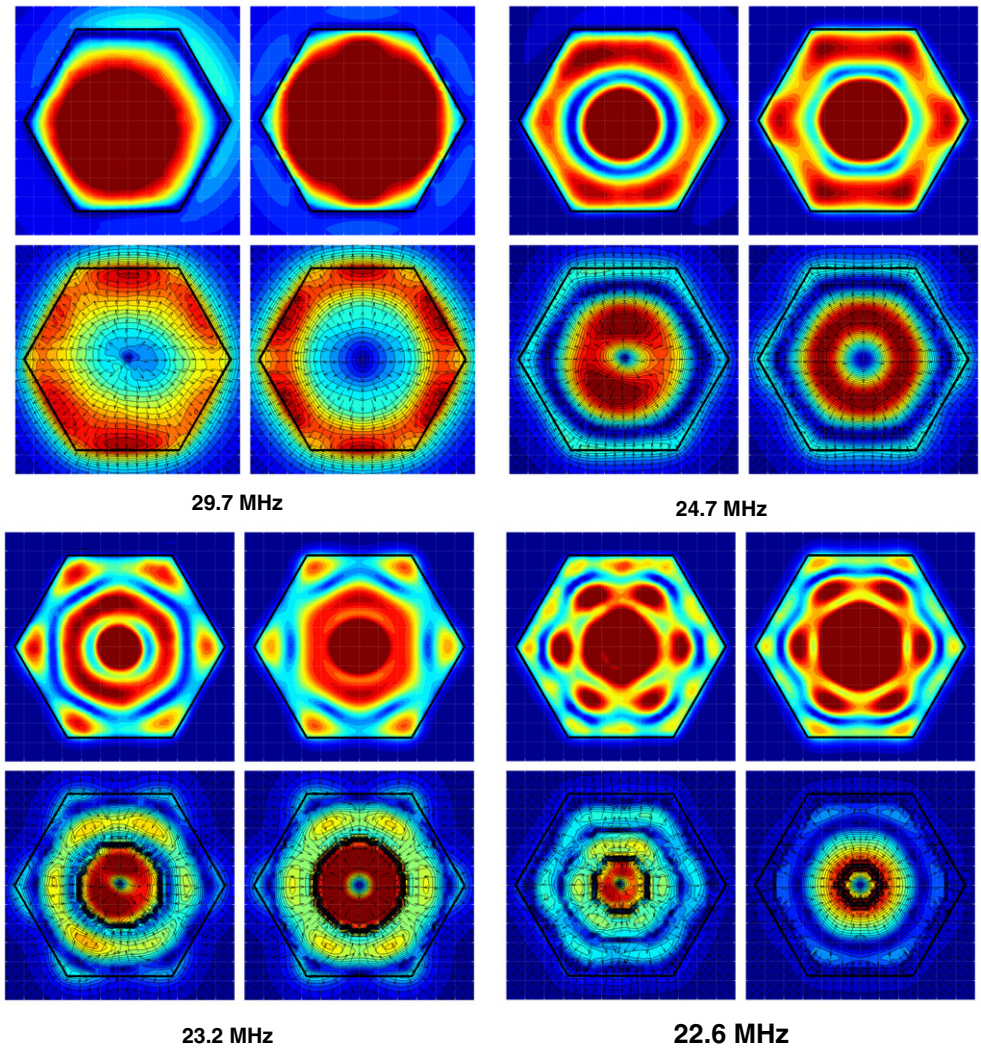

Figure 7. Comparison of measured and modelled resonant field patterns for the hexagonal prism sample. In each frequency group, the left frames are the measured patterns and the right frames are calculated. The upper pair of frames in each case shows the axial field amplitude, $|H_z|$, whereas the lower pair shows the radial field amplitude, $|H_{\rm rad}|$, whose direction is shown by the arrows.

In the left-hand column of figure 6, we show the field patterns calculated using the analytical theory of section 3.2, along with the periodic boundary conditions discussed there, implemented for the situation when the source was taken to be 20 mm behind the rear face of the prism and the wavevector sum in (5) truncated at a spatial frequency corresponding to the roll diameter. First, we note that this model does not produce a result at the highest frequency. Here $\mu_z \approx 0$, so there is an extremely large mismatch between the medium and the vacuum, and hence little field penetration. Thus the predicted transmission in this frequency region is essentially zero. The correlation between the other calculated and measured patterns is better than when the source lies 5 mm behind the prism, and we can clearly see that the basic structure of the field patterns is correctly produced. However, the agreement is not particularly good: overall, the features are rather smaller and sharper than those observed.

In the right-hand column are the results of the numerical simulation, again for the case when the source is 20 mm behind the prism. Here we see a much improved agreement between the model and the measured data: not only is the basic structure of the patterns given correctly, but also the size and shape of the high-intensity regions are well described. This model is able to calculate the correct pattern at the high-frequency end (figure 6(a), 28.5 MHz). Between the two highest resonances, however, some extra structure was calculated, except when a plane wave source was used. At the lower frequencies, below 25 MHz, the agreement between the measured and calculated field patterns is extremely good, and the whole progression from one pattern to another down and through the resonance frequency is correctly described by the numerical simulation. The results are shown for 24.7, 23.65, 23.25 and 22.50 MHz as figures 6(b)–(d), respectively.

4.2.2. The hexagonal prism. Secondly, we consider the data for the hexagonal prism, and take into account both the axial and radial fields. As we have described previously [12], at the highest frequency, 29.7 MHz, we observe a simple drum-head-like resonance, with H_z being maximum at the centre and zero at the edges of the prism. Conversely, the radial field is zero at the centre and maximum at the edges, and points uniformly outwards. As the frequency is reduced, the intensity fades until the next resonance at 24.7 MHz, where we observe a central peak and a ring of intensity in which the sign of H_z is reversed. In the radial field, we see the complementary pattern. As the frequency is further reduced, additional 'rings' of intensity, modulated by the hexagonal symmetry of the prism, appear. The results are shown in figure 7 as the left-hand frames in each set of data.

The right-hand frames of the data sets in figure 7 show the results of the numerical simulation, again with the source placed 20 mm behind the prism, as described in the previous section. It is clear that the agreement between the measured patterns and the simulated results is extremely good, both for the axial and radial field components. As for the square prism, in the high-frequency regime between the first two resonances (at 29.7 and 24.7) the numerical simulation shows additional structure that is not observed in the measurements. As pointed out above, this region is better described by simulations using a plane wave source rather than a finite-sized loop source. As the frequency is reduced towards the resonance of the individual rolls, however, the sequence of patterns and the progression from one to another is well described by the numerical simulation.

5. Discussion

We have shown above that a numerical simulation based on an effective medium description of a magnetic metamaterial is able to give a very good description of the observed spatial resonances in the field patterns around the material samples. However, this was achieved by modifying the actual experimental layout: with the field source in its correct position, additional structure was present in the calculations that did not appear in the measurements. Indeed, at the high-frequency end of the negative permeability regime, good results were obtained using a model excited by a plane wave rather than a small loop source. This indicated that high spatial frequency components arising from the finite size of the source continued to be present in the calculation, although they were not observed in the measurements. Clearly, spatial frequencies greater than that set by the unit cell cannot be sustained in the real material, but are present in the model—there is no cutoff mechanism in an effective medium model. To some extent, this restriction on high spatial frequencies can be simulated by moving the source further away from the sample, to a distance several times the source diameter, so that the highest spatial components are attenuated before impinging on the material. As shown above, this

approach has been very successful in the lower-frequency regime, but less so between the first two resonances; here the plane wave excitation (i.e. launching a uniform magnetic field in the model) gives the best result.

We have also considered an analytical approach within the effective medium framework, similar to that outlined in [11]. There, it was shown that s-polarized radiation whose wavevector lies in the xz plane propagates through an anisotropic magnetic medium according to the relation (2). This model describes the behaviour on resonance well, but predicts finer and more detailed structure that that observed at higher frequency. Indeed, there is good agreement between the analytical models and the numerical model when the source is kept small and close to the material. Our attempts to impose a spatial frequency cutoff in the analytical models (for example, by constraining the upper limit of integration in (5)) have been partially successful. The pattern details are indeed smeared out, and the characteristic features of the spatial resonances are reproduced, but the details of the patterns are not correct. Nevertheless, this simple model gives a surprisingly good account of the experiments.

In [12] we analysed these patterns by appealing to the dispersion relation (7) that relates the propagation wavevectors k_x and k_z via the permeability μ. We argued that the high-frequency resonance was characteristic of $\mu = 0$, and the more complex patterns at lower frequency arose when the combination of the wavevectors and permeability were such as to permit the prism to resonate. By determining the appropriate wavevectors from the dimensions of the prism and the resonant patterns, and deriving the permeability using (7), we calculated that the effective packing fraction F was very close to that for the hexagonal structure. This, combined with the consistency of the field patterns, reassured us that the patterns did indeed arise from resonances of the prism rather than being due to specific values of μ, such as $\mu = -1$. The present simulations reinforce that view: the patterns that are observed in the measurements arise when the fields inside the prism are strongest, i.e. at a resonance, and the axial and radial field patterns complement each other, showing that the field direction in the resonances rotates from the centre to the periphery, with an increasing number of turns as the frequency is reduced.

An alternate description of the Swiss Roll medium can be built up by considering the material to consist of an array of coupled resonators (the individual rolls), with magnetic coupling between each roll [29]. It is then possible to write the currents in each of the N elements, denoted as a vector I of length N, as a response to an exciting voltage V through the $N \times N$ impedance matrix Z, whose elements are the self- and mutual-inductances of the elements, the coupling coefficients above. This has been carried out by Zhuromskyy and co-workers [30], using data extracted from a linear array of these rolls [29], and the response of a hexagonal prism as a function of frequency was calculated. This calculation showed very similar features to those described here. In particular, as the frequency is reduced from well above f_0, a first, uniform resonance is predicted. As the frequency is reduced, the intensity falls, rising again at the next resonance; this has the central peak and a further ring of intensity, as seen in our hexagonal prism at 24.7 MHz. There is no structure in the pattern between these two resonances. Similarly, no extra structure is predicted between here and the next resonance, corresponding to the measured pattern at 23.2 MHz. Thereafter, however, much detailed structure is predicted: indeed, this persists below f_0, and this is not observed experimentally. In addition, we note that the calculated resonant frequencies, f/f_0, are different from those observed; this is surprising because the fully populated $N \times N$ impedance matrix was used in the calculation, and the coupling coefficients, taken from [29], were measured for the same Swiss Rolls as used here.

Thus, the situation regarding additional structure is reversed: whereas in the effective medium model this appears at the higher frequencies and the behaviour near f_0 is correctly predicted, in the coupled resonator approach the reverse is true. It is also interesting to note that a calculation of the present effective medium model, but using a plane wave excitation

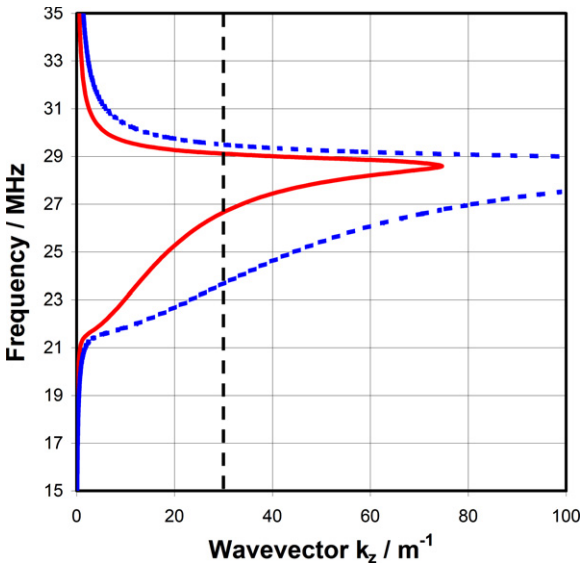

Figure 8. Dispersion curves of frequency versus k_z plotted for $k_x = 5\pi$ (red full line) and 12π (blue dotted line), corresponding to the two limiting values imposed by the roll diameter and the sample size. The dashed line corresponds to the prism thickness being half a wavelength.

rather than a current loop, contains just the resonances at high frequency without the additional structure, but fails near f_0.

A possible explanation for these observation may be seen by considering the dispersion relation (3), which is plotted over the frequency region of interest as figure 8 for two values of the transverse wavevector, k_x, corresponding to the prism size and to the element size. This figure shows that, at a given frequency, a higher k_x demands higher k_z. However, one might expect that the effective medium models would not be accurate for very large k_z, especially for those values corresponding to wavelengths much smaller than the thickness of the prism, i.e. $k_z \sim 50$ or $\pi/0.06$, shown as the dashed vertical line in figure 8.

Although the effective medium can certainly support large k_z, the actual Swiss Rolls probably cannot: no variations in amplitude or phase were observed along the length of 200 mm long rolls excited by a loop at one end, as was done in [10]. The impact of such a restriction is that the effective medium model is good for the lower k_z, and hence for the lower frequencies, but breaks down at higher frequencies when there is no mechanism within the model to restrict the k_z and hence the k_x. The converse appears to be the case for the coupled resonator description.

We see therefore that neither model is perfect. Both predict the existence of resonant field patterns, and correctly calculate the form of those patterns. The evolution of the behaviour with frequency is accompanied in the models by additional structure not observed in practice. In the effective medium model, this occurs at high frequency, and shows that the effect of high spatial frequencies when μ is modest but negative is overestimated. However, we emphasize that the sequence of resonances between 24.7 MHz and $f_0 = 21.6$ MHz is correctly predicted by the effective medium model in both samples, as is the progression from one resonant pattern to the next. Accordingly, we feel that the use of an effective medium picture is justified, provided that the spatial frequency defined by the size of the metamaterial structure is not approached.

Finally, because the wavelength of electromagnetic radiation at these frequencies is so long compared to any length scale in the experiment, we expect the electric and magnetic fields to be essentially independent of one another. Accordingly, an equivalent dielectric model, with the same dispersion parameters but with an electric dipole excitation, should show the same results. This situation, of course, corresponds to the better known plasmon resonances, but on

an interface that lies between a dielectric (ε positive) and a metal (ε negative). We have carried out the MWS calculations for such a system, and indeed find that the results for the electric field are the same as those for the magnetic system. Accordingly, we can think of the resonances that we measure in the field patterns as being due to magnetic plasmons [33].

In conclusion, we have measured and modelled the field patterns around prisms of magnetic metamaterial; these are a series of resonances, increasing in complexity as the fundamental frequency f_0 of the metamaterial elements is approached from above. Provided that the excitation in the model is restricted to low spatial frequencies, excellent agreement between experiment and the effective medium description is obtained.

Acknowledgments

Support from the UK Engineering and Physical Sciences Research Council (EPSRC) and from the European Commission (EC) Information Society Technologies (IST) program DALHM is gratefully acknowledged. JVH thanks Philips Medical Systems for research grant support.

References

[1] Pendry J B, Holden A J, Stewart W J and Youngs I 1996 *Phys. Rev. Lett.* **76** 4773
[2] Pendry J B, Holden A J, Robbins D J and Stewart W J 1998 *J. Phys.: Condens. Matter* **10** 4785
[3] Pendry J B, Holden A J, Robbins D J and Stewart W J 1999 *IEEE Trans. Microw. Theory Tech.* **47** 2075
[4] Smith D R, Padilla W J, Vier D C, Nemat-Nasser S C and Schultz S 2000 *Phys. Rev. Lett.* **84** 4184
[5] Shelby R A, Smith D R and Schultz S 2001 *Science* **292** 77
[6] Parazzoli C G, Greegor R B, Li K, Koltenbah B E C and Tanielian M 2003 *Phys. Rev. Lett.* **90** 107401
[7] Smith D R, Pendry J B and Wiltshire M C K 2004 *Science* **305** 788
[8] Starr A F, Rye P M, Smith D R and Nemat-Nasser S 2004 *Phys. Rev.* B **70** 113102
[9] Smith D R, Schultz S, Markos P and Soukoulis C M 2002 *Phys. Rev.* B **65** 195104
[10] Wiltshire M C K, Pendry J B, Young I R, Larkman D J, Gilderdale D J and Hajnal J V 2001 *Science* **291** 849
[11] Wiltshire M C K, Hajnal J V, Pendry J B, Edwards D J and Stevens C J 2003 *Opt. Express* **11** 709
[12] Wiltshire M C K, Hajnal J V, Pendry J B and Edwards D J 2004 *27th ESA Antenna Technology Workshop on Innovative Periodic Antennas: Electromagnetic Bandgap, Left-handed Materials, Fractal and Frequency Selective Surfaces (Santiago de Compostela, March 2004)* pp 31–7
[13] Pendry J B 2000 *Phys. Rev. Lett.* **85** 3966
[14] Grbic A and Eleftheriades G V 2004 *Phys. Rev. Lett.* **92** 117403
[15] Fang N, Lee H, Sun C and Zhang X 2005 *Science* **308** 534
[16] Blaikie R J and Melville D O S 2005 *J. Opt. A: Pure Appl. Opt.* **7** S176
[17] Melville D O S and Blaikie R J 2005 *Opt. Express* **13** 2127
[18] Wiltshire M C K, Pendry J B and Hajnal J V 2006 *J. Phys.: Condens. Matter* **18** L315
[19] Smith D R and Schurig D 2003 *Phys. Rev. Lett.* **90** 077405
[20] Smith D R, Kolinko P and Schurig D 2004 *J. Opt. Soc. Am.* B **21** 1032
[21] Mock J J, Barbic M, Smith D R, Schultz D A and Schultz S 2002 *J. Chem. Phys.* **116** 6755
[22] Balmain K G 1964 *IEEE Trans. Antennas Propag.* **12** 605
[23] Balmain K G, Luttgen A A E and Kremer P C 2002 *IEEE Attennas Wireless Propag. Lett.* **1** 146
[24] Wiltshire M C K, Pendry J R, Hajnal J V and Edwards D J 2003 *IEE Seminar on Metamaterials for Microwave and (sub) Millimetre Wave Applications (London, Dec. 2003)* Paper 13
[25] Wiltshire M C K, Yannopapas V and Pendry J B 2004 *PIERS: Progress in Electromagnetics Research Symposium (Pisa, March 2004)*
[26] Shamonina E, Kalinin V A, Ringhofer K H and Solymar L 2002 *Electron. Lett.* **38** 371
[27] Shamonina E, Kalinin V A, Ringhofer K H and Solymar L 2002 *J. Appl. Phys.* **92** 6252
[28] Wiltshire M C K, Shamonina E, Young I R and Solymar L 2003 *Electron. Lett.* **39** 215
[29] Wiltshire M C K, Shamonina E, Young I R and Solymar L 2004 *J. Appl. Phys.* **95** 4488
[30] Zhuromskyy O, Shamonina E and Solymar L 2005 *Opt. Express* **13** 9299
[31] Wiltshire M C K 2007 *Phys. Status Solidi* b **244** 1227
[32] Panofsky W K H and Phillips M 1964 *Classical Electricity and Magnetism* 2nd edn (Reading, MA: Addison-Wesley) p 90 (Section 5.8)
[33] Pendry J B and O'Brien S 2002 *J. Phys.: Condens. Matter* **14** 7409